

# An Old but Lively Nanomaterial: Exploiting Carbon Black for the Synthesis of Advanced Materials

M. Alfe<sup>1\*</sup>, V. Gargiulo<sup>1</sup>, R. Di Capua<sup>2</sup>

<sup>1</sup>Institute for Research on Combustion (IRC-CNR), Naples, Italy

<sup>2</sup>Department of Physics “E. Pancini” University of Naples Federico II, and CNR-SPIN, Naples, Italy

## Article info

*Received:*  
12 December 2018

*Received in revised form:*  
16 February 2019

*Accepted:*  
8 April 2019

## Keywords:

Carbon black  
Advanced materials  
Graphene-related materials

## Abstract

Carbon black (CB) is an old-concept but versatile carbonaceous material prone to be structurally and chemically modified under quite mild wet conditions. Recently, we exploited the potentiality of CB for the production of a highly varied array of advanced materials with applications in energetics, water remediation and sensoristic. The proposed approaches are devised to meet specific needs: low production costs, scalable synthetic approaches, flexibility i.e. easy tuning of chemico-physical properties of the carbon-based advanced materials. Two main approaches have been exploited: modification of CB at the surface and highly CB de-structuration. The former approach allows obtaining highly homogenous CB-modified nanoparticles (around 160 nm) with tunable surface properties (hydrophilicity, typology of functional groups and surface charge density, pore size distribution), supports for ionic liquid (SILP) and composites (carbon-iron oxide). The latter approach exploiting a top-down demolition of CB produces a highly versatile graphene related material (GRM), made up by stacked short graphene-like layers (GL) particularly suitable for advanced composites synthesis and ultrathin carbon-based films production.

## 1. Introduction

Carbon black (CB) is a commercial carbonaceous material derived from a highly-controlled pyrolysis process (furnace black) or thermal decomposition (thermal black) of hydrocarbons and/or heavy aromatic oils (basically petrochemical feedstocks). The different manufacture processes designate the different kinds of CB with specific chemico-physical properties [1].

Broadly speaking, at the nanoscale level CB is composed almost exclusively of randomly stacked, concentrically arranged, sheets of condensed aromatic ring systems (i.e. graphene layers) oriented around growth centers to form almost spherical primary particles (10–300 nm). Primary particles are fused into grape-like shaped aggregates (acini-form aggregates, usually less than 500 nm) thus representing the discrete, dispersible CB smallest unit. Aggregates clustered in the so-called agglomerates (Fig. 1).

CB are usually highly agglomerated, with 10 to 1000 aggregates per agglomerate. The three-dimensional configuration of the CB aggregates results in varied but usually large surfaces areas (SA) (between 5–200 m<sup>2</sup>/g). The size of the primary particle and the degree of aggregation differentiate the grades of carbon blacks [2]. In turn, these physical characteristics address the commercial use of the specific CB, that are commonly used as reinforcing agent or conductivity enhancer in rubber and as components in inks and coatings [2]. Advanced and challenging application are emerging: CB have been proposed as sensitive components in electrochemical sensors [3], as counter electrodes of dye-sensitized solar cells [4], as materials to produce photocatalysts [5] and composites with heat insulating properties [6], as electrically conductive fabrics for wearable heating applications [7], and as materials to improve the physical properties (i.e. electrical conductivity) of construction materials [8–9].

\*Corresponding author. E-mail: [alfe@irc.cnr.it](mailto:alfe@irc.cnr.it)

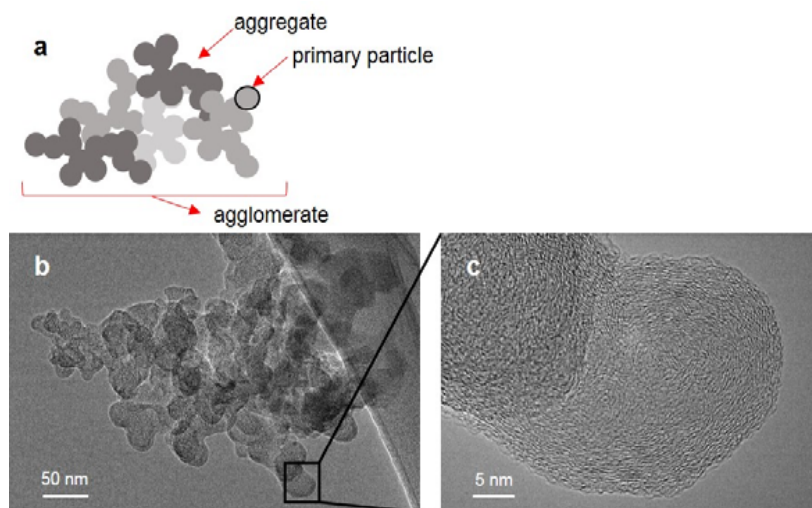


Fig. 1. Structure of CB (a), at micro (b) and nanoscale (c) level.

CB are composed almost exclusively by elemental carbon (> 95 wt.%) with a variable quantity of hydrogen, oxygen, and sulfur (less than 1% each); usually the hydrogen to carbon atomic ratio (H/C) is less than 0.05 [2, 10]. Trace amounts of organic compounds (polycyclic aromatic hydrocarbons and aliphatic/aromatic hydrocarbons) and inorganic impurities (salts of alkali and alkaline earth metals) as manufacturing residuals can be also found [10].

In our approach, we explored the potentiality of CB for the production of a highly varied array of advanced materials. The proposed approaches intersect and face the continuous need of low cost and scalable methods for an easy tuning of the relevant chemico-physical properties of carbon-based materials. We choose, as case study, a CB N110 type (furnace black), purchased from by Sid Richardson Carbon Co. The density of this

CB at 25 °C is 1.8 g/mL and the inorganic content is negligible (less than 0.1 wt. %, evaluated at 800 °C). This N110 CB is a mesoporous material with a SA of 139 m<sup>2</sup>/g. As expected, its microstructure is organized in chain-like aggregates [11–12] of almost spherical primary particles (15–20 nm diameter). The hydrodynamic diameters of the aggregates, measured by Dynamic Light Scattering (DLS), is 160±20 nm. The CB nanostructure consisted of stacked graphene layers arranged in a turbostratic fashion typical of a disordered carbon. A concentric organization of the graphenic layers is discernible in the best structured areas and extends throughout each primary particle (Fig. 1).

Two main approaches have been exploited to produce CB derived materials designed for specific technological applications (Fig. 2):

- i) modification of CB at the surface;
- ii) highly CB deconstruction.

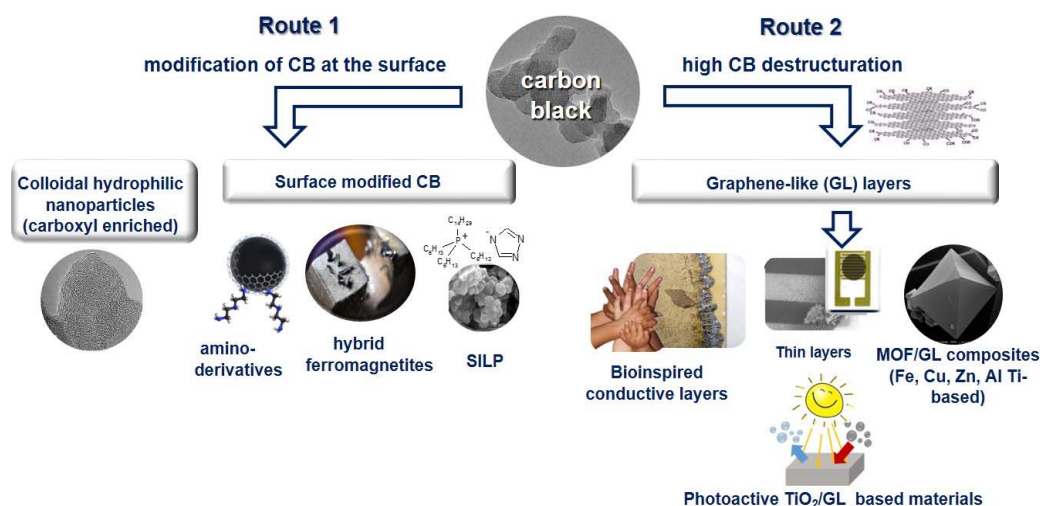


Fig. 2. New-concept materials from CB.

The former approach allows obtaining highly homogenous CB-modified nanoparticles (hydrodynamic diameter around 160 nm) with tunable surface properties (hydrophilicity, typology of functional groups and surface charge density, SA and pore size distribution), suitable also to serve as supports for ionic liquid (SILP) and for the growth of magnetic iron oxide. The latter approach leads to a top-down demolition of CB in highly versatile graphene related material (GRM), made up by water-stable stacked short graphene-like layers (GL) suitable as building blocks for advanced composites synthesis and ultrathin carbon-based films production.

The huge and varied pool of materials arising from CB processing (Fig. 2) originates from the possibility offered by CB to be structurally and chemically modified under quite mild wet conditions.

In the following details on the synthetic approaches, the structural characteristics and potential applications of the developed materials are reported.

## 2. Results and discussion

### 2.1. Modification of CB at the surface

#### 2.1.1. Colloidal hydrophilic nanoparticles (carboxyl enriched) [12]

Colloidal hydrophilic nanoparticles (HNPs) with uniform size have been produced through a very simple oxidative treatment of CB N110 with hot nitric acid [12]. The wet-chemistry treatment, performed at different reaction times (4, 15, and 24 h), generates nanoparticles, herein named HNP-1, HNP-2, HNP-3, respectively, with an increasing oxygen content (from 0.59 wt.% in neat CB up to 34.8 wt.% in HNP-3). The HNPs bear on the surface a variable number of oxygen functional groups (mainly carboxylic groups), enhancing their hydrophilicity and colloidal stability [12]. The total number of oxygen functional groups varies from  $1.56 \pm 0.10$  mmol/g in HNP-1 to  $2.25 \pm 0.08$  mmol/g in HNP-3. Interestingly, the acid treatment up to 24 h does not alter the graphitic planes arrangements but favors the development of a high amount of micro and mesopores [12] enhancing the surface area from  $139 \text{ m}^2/\text{g}$  (raw CB) to  $323 \text{ m}^2/\text{g}$  (HNP-3). Moreover, the hydrodynamic diameter of the aggregate and primary particles keeps constant (around  $165 \pm 10$  nm). All of the HNPs exhibit a good colloidal stability in water in a wide pH range (from 4 to 12) [12].

HNPs are found to be particularly suitable for wastewater remediation from heavy metal pollution. Their capability to reversibly catch heavy metals ions was probed using cadmium as case study [12]. All the HNPs exhibit an appreciable adsorption capacity of cadmium at different temperatures ( $10\text{--}60$  °C) and in a wide range of pH (2–6).

It was also found that the concentration of active sites (specifically carboxylic functional groups) on the HNP surface well correlate with the cadmium adsorption capacity. Since the most important parameter for water depuration is the actual adsorption capacity close to the allowed discharge limit, by fixing the limit for sewage discharge at 0.2 mg/L (accordingly with the current regulations in Italy), it was established that the cadmium adsorption capacity at 20 °C and pH 3.5 (most of the cadmium waste waters are acidic) was 1.06 mg/g for HNP-1 reaching 1.62 and 3.84 mg/g for HNP-2 and HNP-3, respectively [12].

The comparison with other carbon-based sorbents reported by pertinent literature showed performances comparable or superior with respect to commercial activated carbons (even those oxidized), ashes, and residual solids while being similar or far lower compared to specific sorbents from bio sources (activated char) or polyacrylonitrile (PAN) fibers [12].

To overcome the difficulties in the separation of HNPs from their colloidal water suspension and taking advantage of the oxygen functional groups borne by the HNP particles, a very simple coating of silica particles was further achieved without losing in heavy metal adsorption performances [12]. The HNP particles supported over silica allowed easy filterability from wastewater for  $\text{pH} > 2.5$  (where the high HNPs colloidal stability hinders a simple filtration to isolate the particles from the decontaminated waters) paving the way for a feasible use of these sorbents for heavy metal adsorption in commercial units [12].

#### 2.1.2. Surface modified CB (Carboxyl and amino-derivates, $\text{CB}/\text{Fe}_3\text{O}_4$ , Supported Ionic Liquids) [13–16]

$\text{CO}_2$  adsorption by solid sorbents is one of the most promising options for post-combustion  $\text{CO}_2$  capture strategies [17] since it requires reduced energy consumption for regeneration and offers great capacity, selectivity, and ease of handling. A competitive sorbent for  $\text{CO}_2$  capture applications should i) be economically convenient (both in the

synthesis and in the regeneration steps); ii) be able to selectively interact with CO<sub>2</sub> over the other flue gas components, and (iii) be stable (chemically and mechanically) to undergo repeated CO<sub>2</sub> sorption and desorption cycles over a wide range of temperatures and pressures [18]. Overall, materials with a distinctive surface chemistry and porosity find large applications in CCS technologies [17–20]. Ferric oxide nanoparticles are a cost-effective CO<sub>2</sub> sorbent thanks to the instaurations of favorable acid–base interactions (Lewis type) between the active sites exposed at the surface (coordinatively unsaturated metal and O sites) and the CO<sub>2</sub> molecule, leading to the formation of adsorbed carbonates, bicarbonates and carboxylates, as well as bent CO<sub>2</sub> species [21–23]. The efficient use of ferric oxide under the post-combustion CO<sub>2</sub> capture conditions is hampered by the tendency of magnetite particles to agglomerate. The dispersion of ferric oxide nanoparticles over a carbonaceous matrix was proven to be a promising strategy to overcome this shortcoming [22–23]. In this framework we produced a series of CB modified at the surface to serve as sorbent for CO<sub>2</sub> capture applications by coating CB with different amounts of iron oxide [13].

Composite materials were synthesized in a one-pot synthetic approach by exploiting a co-precipitation strategy allowing the iron oxide particles to form in presence of CB. A series of five CB/FM composites was obtained by varying the CB to FM ratio. The one-pot strategy was proved to allow a homogeneous incorporation of both the carbonaceous material and the iron oxide particles into the composites. All the five investigated materials exhibited comparable SA (around 150 m<sup>2</sup>/g), and, as expected, the increase of CB loading in the CB/FM composite shifts the pore size distribution from the porosity typical of FM (20–50 Angstrom) toward those typical of the CB (broadly centered around 200 angstroms) [13]. The experimental campaign conducted in a lab-scale fixed bed reactor under dynamic conditions established that the CO<sub>2</sub> uptake of the CB/FM composites increases with respect to the pure FM when the amount of CB in the composite ranges between 14.3 and 60 wt.%. This indicates that a synergistic effect between the role of the material surface area (physisorption) and the presence of the active phase toward CO<sub>2</sub> sorption (chemisorption) has been reached.

The best adsorbing composite (50 wt.% of CB load, 16.5 mg CO<sub>2</sub>/g) was produced on a larger scale and tested in a prototypal sound assisted flu-

idization apparatus [13]. Under the sound assisted fluidization conditions the CO<sub>2</sub> uptake was considerably enhanced up to about 20 mg CO<sub>2</sub>/g. Several CO<sub>2</sub> adsorption and desorption cycles without losing in performances, also demonstrated the potentiality of the CB/FM composites for applications in practical units. It has to be underlined that the characteristic CO<sub>2</sub> adsorption/desorption times are comparable (11 min) paving the way to operate cyclically in two interconnected fluidized bed [13]. The possibility to exploit the magnetic properties of the composites are currently under study.

The performances of the CB/FM (50 wt.%) composite were investigated also performing a thoroughly thermodynamic characterization under dynamic conditions [14]. More in detail, the CO<sub>2</sub> adsorption data collected under isothermal conditions (18–150 °C) and with CO<sub>2</sub> partial pressure ranging between 0.5–20 vol.% [14] showed that adsorption temperature and pressure have opposite effect on the thermodynamics of the process i.e. the CO<sub>2</sub> adsorption capacity increases with increasing pressure and decreases with increasing temperature. The Freundlich and Toth models resulted to better fit the CO<sub>2</sub> adsorption process suggesting the establishing of a multilayer process characterized by a heterogeneous surface binding. The CO<sub>2</sub> adsorption on CB/FM was found to be a spontaneous and exothermic process based neither on purely physisorption nor on purely chemisorption.

In our experimentation on CB/FM, the surface area of the carbonaceous support and, more specifically the distribution of micro and mesopores, was proven to play a relevant role. To go deep into this important issue, raw CB has been worked out to expose a different porosity (and surface properties) and has been used as solid support for different typology of CO<sub>2</sub> active phases [13–16]. CB surface area was increased by oxidation (up to 323 m<sup>2</sup>/g) thus increasing the micropores/mesopores ratio. The oxidized CB (above named HNP-3 or, for sake of brevity CB<sub>ox</sub>) was: i) used as it is; ii) thermally treated; iii) grafted with amino-groups, iv) coated with iron oxide particles CB<sub>ox</sub>/FM (50 wt.%); v) impregnated with the basic ionic liquid (IL) trihexyl(tetradecyl)phosphonium tri-azole ([P66614][Triz]) CB<sub>ox</sub>/IL. In the latter case, also the IL impregnated CB (CB/IL) has been produced for comparison [15]. All the CB-based adsorbents exhibit good thermal stability (up to 600 °C in the case of oxidized material, up to 200 °C in the case of amino-functionalized material and IL-supported sorbent and up to 500 °C in the case of iron oxide

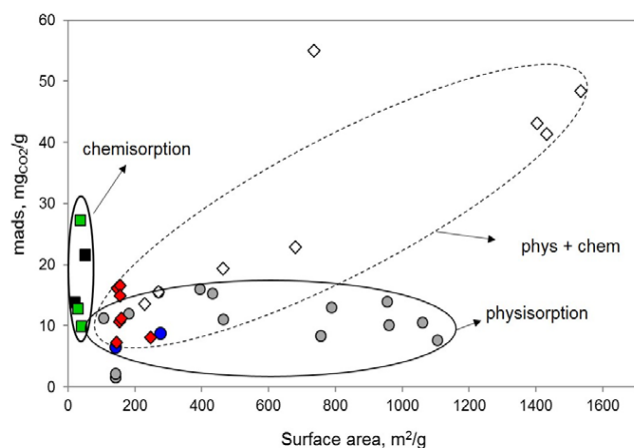


Fig. 3. Plot of  $m_{\text{ads}}$  vs. surface area (lab-scale fixed bed micro-reactor, %  $\text{CO}_2$  in  $\text{N}_2$ : 3–10). ■ (green squares):  $\text{CB}_{\text{ox}}\text{-NH}_2$ ,  $\text{CB-IL}$  and  $\text{CB}_{\text{ox}}\text{-IL}$ ; ◆ (red diamonds):  $\text{CB/FM}$  at different  $\text{CB:F}$ M ratio; ● (blue circles):  $\text{CB}_{\text{ox}}/\text{FM}$  and  $\text{CB}$ ; data are contrasted with literature available sorbents working in the same conditions and grouped in physisorbents (●, grey circles), chemisorbents (■) and mixed behavior (physisorbents + chemisorbents, ◆). Adapted from [16].

containing composites) and a good variability in terms of surface areas and pore size distributions [15–16]. The  $\text{CO}_2$  capture performances, evaluated with tests performed simulating real post-combustion working conditions ( $\text{CO}_2$  3–10% vol. and atmospheric pressure) in a lab-scale fixed bed micro-reactor [15], highlighted the different nature of the sorption (physisorption, chemisorption or an intermediate nature) [16], as reported in Fig. 3.

As concerns the effect of textural properties of the carbonaceous support, our experimentation indicated that the microporosity greatly limits the accessibility of  $\text{CO}_2$  toward the sorbing absorbing phase (IL or FM) that is clogged into the micropores, lowering the number of available binding sites for  $\text{CO}_2$  [15].

### 3. Highly CB deconstruction

#### 3.1. Graphene-like (GL) layers and ultrathin (GL) films [24–27]

One of the most fascinating CB potentiality is the possibility to obtain a highly versatile graphene related material (GRM) by its deconstruction. The CB-derived GRM is made up by stacked short graphenic fragments (here in the following graphene-like layers, GL) and it is obtained through a two steps oxidation/reduction approach [24–26] allowing scalability and poten-

tially large-amount production at reduced costs. Differently from the well-known reduced graphene oxide (rGO) obtained by similar approaches, the GL layers present intact graphenic basal planes (whereas the rGO present holes and defects) that are important to guarantee the electrical conductivity. Infrared and X-ray photoemission spectroscopy inspections indicated that the edges of the GL basal planes are decorated mainly by oxygen functional groups (mainly carboxylic and carbonyl groups) [24–25]. Coulometric–potentiometric titration in the pH range  $2.7 < \text{pH} < 7$  identified two functional groups classes in the carboxylate region ( $\text{pK} 2.0\text{--}5.0$ ) with  $\text{pK}_a = 3.40 \pm 0.05$  (number of sites =  $900 \pm 30$  mmol/g) and  $\text{pK}_a = 5.5 \pm 0.1$  (number of sites =  $240 \pm 30$  mmol/g, mainly lactones and carboxylic anhydride groups that tend to hydrolyze in the presence of acids and bases) [25]. The presence of such a complex variety of oxygen functional groups gives to the GL layers an exceptional colloidal stability over a wide pH range (3–14).

GL layers exhibit a peculiar self-assembling behavior when dried on surfaces, arranging in different morphologies (ranging from atomically flat to patterned surface) as a consequence of the suspension pH, surface roughness and GL surface chemistry [25–27]. I-V measurements showed linear responses implying an Ohmic behavior of GL films. The conductivity of a GL film of around 20 nm height, estimated by the classical four-probe van der Pauw configuration [28] was  $2.5 \pm 0.3 \cdot 10^{-2}$  S/cm [24].

The good conductivity combined with the easy tunable GL morphologic arrangement as films was found to be relevant for sensoristic applications in alcohol detection [27] in the wake of the emerging request of low-cost, eco-compatible VOCs sensors for the air quality monitoring working at room temperature [29]. The sensing performances of GL layers-based prototypal chemiresistive devices against alcohols (ethanol and n-butanol) detection were evaluated at atmospheric pressure, room temperature and dried atmosphere, in the concentration range 0–100 ppm. GL layers exhibited a response toward ethanol, expressed as normalized relative variation of conductance, around 3% and toward n-butanol around 0.5% (Fig. 4) [27]. The comparison of the experimental results with those reported by literature showed that GL films are promising candidate for the detection of low concentration of ethanol at room temperature [27].

In Fig. 4, the GL layers response (in terms of conductance variation) is compared to that of its oxidized precursor  $\text{GL}_{\text{ox}}$  highlighting how the

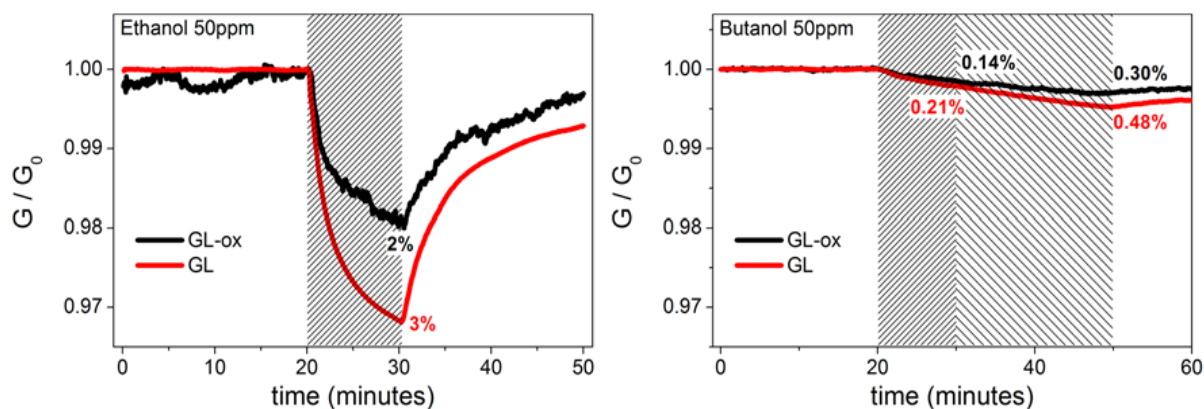


Fig. 4. Comparison between the response of the chemiresistive device based on  $GL_{ox}$  (black curve) and GL films (red curve) toward ethanol (right panel) and n-butanol (left panel). Adapted from [27].

enhanced conductivity of GL toward  $GL_{ox}$  give rise to a much more efficient paths for the charge carriers arises. The response of the chemiresistive device based on  $GL_{ox}$  exhibited an extremely low SNR ( $< 25$  db) compared to that based on GL films ( $> 45$  db).

The lower sensitivity to n-butanol (Fig. 4) compared to ethanol could be ascribed to the different ability of the analytes to permeate the GL flakes (the analytes have a different steric hindrance), as well as to different chemical affinity to functional groups on the GL layers surfaces. A combined role of morphology and surface chemistry in determining the response to the analytes was assumed as a possible interpretation of experimental evidences. Both features are in principle tunable by acting on the synthesis parameters, forecasting promising perspectives for the improvement and the full control of sensing performances.

Starting on these promising results, preliminary attempts to process GL layers from aqueous suspension in finely controlled paths by means of inkjet printing (IJP) have been performed [30]. The IJP technology permits an efficient use of different functional inks reducing the amount of waste products, and nonflexible and flexible eco-friendly substrates (as paper substrates) [31]. Ethanol chemiresistors have been fabricated by printing GL layers onto glossy paper with interdigitated Cr/Au electrodes [30].

The response toward ethanol (50 ppm, in dry  $N_2$ ) in terms of conductance variation was 1.3%, and intra-substrate reproducibility in terms of surface morphology (macroscopic and microscopic distribution of the printed nanomaterial) and electrical responses (base resistance and conductance variation) was also demonstrated [30]. The possi-

bility to use different substrates (alumina, silicon dioxide) is currently under study to evaluate the chemiresistor inter-substrate reproducibility.

Thanks to their peculiar characteristics, GL layers are also particularly suitable to homogeneously coat non-planar surfaces, including particles ( $TiO_2$ , Silica,  $Al_2O_3$ ) and living cells [32]. The interest in contacting living cells with graphene and GRMs relies in their proven potential antimicrobial and scavenging activities. GL layers have been found to act as inhibitor toward the planktonic growth of *S.aureus* cells also hindering the formation of *S.aureus* biofilms [32]. The presence of GL in the of *S.aureus* cells culture media induces a severe decrease of colony forming units (CFU). These data are in agreement with the antibacterial properties of GRMs, with graphene oxide (GO) being more active than pristine graphene [33]. In order to analyze the interaction between GL layers and the cells, the cell membrane integrity of *S.aureus* cells treated with GL layers was investigated using the LIVE/DEAD assay. Interestingly, at 100  $\mu g/ml$  GL treatment for 24 h, *S.aureus* cells showed no significant difference in viability compared to control, indicating that there is no evidence of cell membrane leakage caused by GL layers. The imaging survey by FE-SEM and AFM microscopies revealed the instauration of an intimate contact between the cells and the GL layers: cells appeared almost covered by the nanomaterial and no mechanical damage of the bacteria was observed confirming the preservation and the integrity of the plasma membrane. These experimental evidences suggested that the GL antimicrobial properties were based mainly on the interaction between GL layers and bacteria surfaces [32], then acting as bacteriostatic agent more than cells toxic agent.

### 3.2. Graphene-like (GL) layers and conductive hybrid materials synthesis [34–38]

The peculiar characteristic of GL layers to establish stable colloidal suspensions after dispersion in water without the use of any surfactant make them particularly suitable for the preparation of a wide array of electrically conductive hybrid materials including intercalated metal organic frameworks MOFs [26, 34], biocompatible interfaces [35–36] and photoactive materials [37–38].

MOFs attracted in the last years a great attention due to interesting structural properties: i) high surface area (up to 4500 m<sup>2</sup>/g); ii) defined porosity; iii) regular structure; iv) easy synthetic routes; v) crystallinity; vi) low density; vii) flexibility and more. [39–40]. The possibility to vary their metallic centers and organic linkers allows to tune their chemico-physical and textural properties making them suitable for a large array of specific applications [40–43]. The electrical properties of MOFs were very rarely studied due to their insulating nature. The preparation of composites combining MOFs and carbon-based materials has been proposed as a solution to overcome the weak points of MOFs and to expand their field of applications [44]. The embedding of conductive graphene-like layers into the structure of copper-based MOF in a one-pot strategy was successfully achieved as possible route to improve MOF conductive properties [26, 34]. Our first experimentation on the well-known copper-based MOF HKUST-1 (also known as MOF-199 or Basolite) demonstrates that the composites were produced incorporating up to 40 wt.% of GL layers kept preserved the characteristic features of pristine HKUST-1 crystal. Moreover, the incorporation of GL layers alters the MOF pore size distribution introducing pores of 6 Angstrom in diameter along the 7–8 Angstrom typical of the HKUST-1 crystal although the surface area of the composites is lower than the HKUST-1 indicating a distortion in the porous structure of the materials. The presence of embedded GL layers induces a non-linear increase of the electrical conductivity up to 5 orders of magnitude when the GL amounts accounts to 40 wt.% in the composites (10<sup>-2</sup> S/m). The above reported approach has been successfully applied in the formulation of MOFs with different metallic centers (Zn, Zn/Cu, Fe, Al, Ti) for practical application as CO<sub>2</sub> sorbents. The peculiar MOF/GL electrical conductivity also paves the way for applications in advanced technological fields as sensors development that are currently under study.

In the manifold of available materials for the production of functional biocompatible interfaces, the human pigment eumelanin (EU) is currently gaining a growing interest. Much efforts are currently devoted to empowering the chemico-physical characteristics of the raw EU, with the aim to fabrication efficient eumelanin-based devices through: i) improvement of EU solubility and processability; ii) improvement of EU low electrical conductivity [45].

Among the different strategies under investigation to improve electrical performances of EU thin films, a clear-cut approach lies in the combination with a suitable conductive counterpart. In this view,  $\pi$ -conjugated systems molecules featuring conducting pathways, appear a key choice in the production of new organic materials for electronic (nano)devices development. Following this approach, a conductive interface was designed and fabricated by an efficient integration of EU and graphene like (GL) layers [35]. The hybrid EUGL was produced allowing EU precursors (5,6-dihydroxyindole (DHI) and/or 5,6-dihydroxyindole-2-carboxylic acid, DHICA [46]) to polymerize in water in presence of suspended GL layers [35–36]. The hybrid material (EU:GL ratio 1:1 wt/wt) was characterized by chemical-physical, electrical and morphological analyses and its biocompatibility was proven toward mammalian cell cultures (Murine Embryonic Stem Cell and Rat Microglial Cell) *in vitro* in view of its potential exploitation as bio-interface [35]. The structural analyses suggested that the actual EUGL composition could be considered as the outcome of quantitative merging of the starting materials (GL layers and EU). The nature of the eumelanin-GL interaction is currently under study: it has been speculated that both covalent bonds and  $\pi$ - $\pi$  stacking are involved, the latter arising from the tendency of GRMs to interact with aromatic systems. Comparative AFM inspection of the morphologies of EU, GL and EUGL thin films indicates a serious modification induced by EU to the atomically flat surface exhibited by GL layers after self-assembling on a flat surface (Fig. 5) and a dramatically improved adhesion behavior to hydrophilic and hydrophobic surfaces [35]. EUGL exhibits an electrical conductivity ( $\sigma$ ) more than four orders of magnitudes greater than that of EU ( $\sigma_{EU} = (3.6 \pm 0.5) \cdot 10^{-8}$  S/cm;  $\sigma_{EUGL} = (9 \pm 2) \cdot 10^{-4}$  S/cm) and a characteristic  $\sigma$  time-decay lower and less pronounced compared to that of EU (such phenomenon is absent in the GL film). The very different  $\sigma$  decays in EU and EUGL also

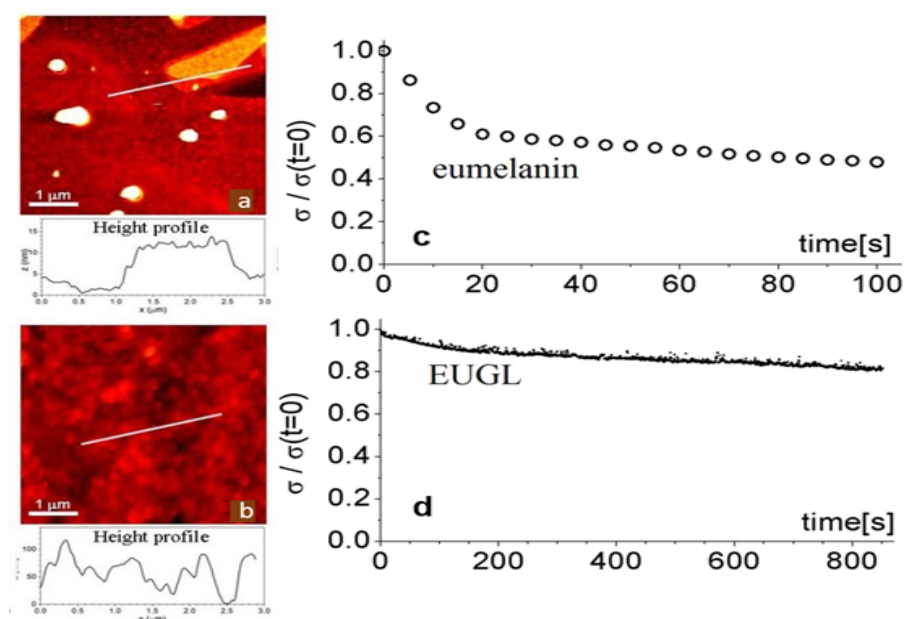


Fig. 5. Non-contact AFM images ( $5 \mu\text{m} \times 5 \mu\text{m}$ ) with corresponding height profile on a line of about  $3 \mu\text{m}$  on: (a) – EU; (b) – EUGL. Time dependent decay of the electrical conductivity on the EU – (c) and EUGL films – (d), at a fixed voltage (100 V for the EU, 100 mV for the EUGL). Adapted from [35].

present a typical double time-scale, a «fast» initial decay, followed by a further slower decrease, suggesting the presence of both ionic and electronic contributions to the electrical transport (Fig. 5) [35].

An experimental campaign involving sophisticated analytical techniques as X-ray photoemission and absorption spectroscopies with synchrotron radiation and solid state nuclear magnetic resonance (ss-NMR) was also performed on EUGL hybrids by exploring different EU to GL mass ratios. This survey allowed to get insights into the interaction between the two conjugate  $\pi$  systems and macroscopic and microscopic electrical behaviors of EU-based hybrids [47].

A detailed investigation on the high frequency electrodynamics (THz region) in GL layers and its biocompatible hybrid EUGL via THz spectroscopy was also performed [36]. A mean field theory is applied to extract direct information on the permittivity and conductivity. Data have been carefully fitted through Drude-Smith theory confirming the conductive nature of the hybrid compounds. Tuning the concentration of the guest material (GL, EU or EUGL) in the KBr pellet, we inferred relevant intrinsic electrodynamic parameters of the materials (EP), such as the complex permittivity and hence the conductivity. The measured values of conductivity are encouraging and open the possibility to employ GL and EUGL hybrids for the development of bio-compatible circuitry and devices working up to the THz range [36].

### 3.3. Graphene-like (GL) layers and photoactive hybrid materials synthesis [37–38]

Heterogeneous photocatalysis has proved to be as an efficient and versatile tool for the degradation of both atmospheric and aquatic organic pollutants [48].  $\text{TiO}_2$  is one of the most studied semiconductor photocatalysts due to its superior intrinsic photocatalytic activity, easy availability, low cost, low toxicity and long-term stability against photo and chemical corrosion [49–50]. The versatile properties of  $\text{TiO}_2$  stimulate a huge literature aimed to improve some characteristics as charge mobility and hindering the electron-hole recombination via charge separation. The synthesis of hybrid materials, in which a suitable material is combined with  $\text{TiO}_2$  (through doping, impregnation, anchoring, etc.) to favor the spatial separation of photogenerated charges is an effective strategy [51]. Among the materials suitable for this approach, GRMs are the most promising ones because of their high electron-trapping ability and chemical stability [52]. GL layers were used to design  $\text{TiO}_2$ -based hybrid photocatalysts by direct growth of  $\text{TiO}_2$  on GL layers in water, followed by calcination [34, 38]. Two different composites ( $\text{TiO}_2/\text{GLP}$  and  $\text{TiO}_2/\text{GLW}$ ) were produced by using GL layers as solid nanoplatelets (dried in air and then suspended in water: GLP) and GL in water suspension (as produced and not dried: GLW) in order to assess the effect of composite morphology on the selective conver-

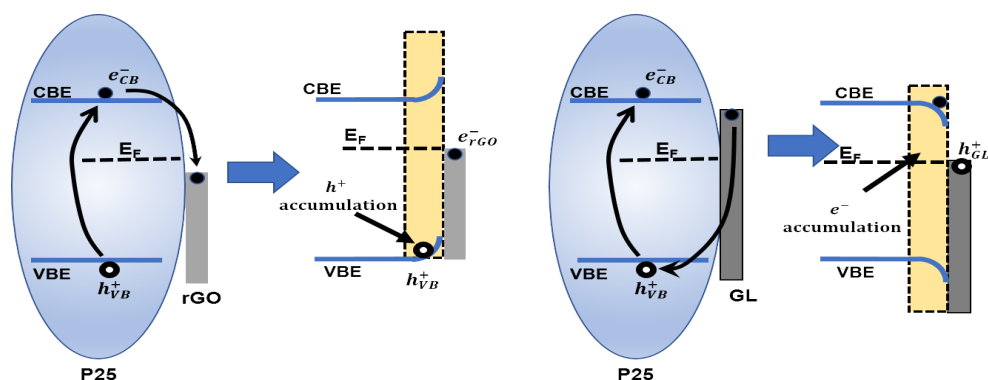


Fig. 6. Pictorial representation of the charge-transfers proposed for  $\text{TiO}_2/\text{rGO}$  (left) and  $\text{TiO}_2/\text{GL}$  (right) composites. CBE and VBE are conduction and valence band, respectively. Yellow regions represent the sub-surface accumulation regions for electrons in P25.

sion of 3-pyridine methanol to 3-pyridine carboxaldehyde and nicotinic acid (vitamin B3), under de-aerated and UV/solar simulated conditions, in the presence of cupric ions [38]. An enhanced photocatalytic activity, with respect to the neat  $\text{TiO}_2$ , has been observed and attributed to the broader variety of stable free-radical species generated, at a given photo-catalyst morphology, within the delocalized  $\pi$ -electron systems. In particular, the enhanced photocatalytic activity and selectivity of  $\text{TiO}_2/\text{GLP}$  (global selectivity 97% compared to 87.3% in the case of neat  $\text{TiO}_2$ ) was attributed both to the broader variety of free-radical species stabilized within the delocalized  $\pi$ -electron systems of the  $\text{TiO}_2/\text{GLP}$  and to a reduction of the hydroxyl radical formation. In the case of  $\text{TiO}_2/\text{GLW}$ , the presence of well dispersed GL layers during  $\text{TiO}_2$  nucleation seems to interfere with the  $\text{TiO}_2$  crystallization process lowering the composite photocatalytic activity, in spite of its higher surface area [38].

With the aim of deepening the understanding of the various factors that can affect the actual charge transfer behavior and heterojunction effects in  $\text{TiO}_2/\text{GL}$  composite, materials containing growing amount (up to 10 wt.%) of GL layers were prepared through a solvothermal approach in presence of  $\text{TiO}_2$  (P25 benchmark) [37]. The composite materials were structurally analyzed by combining standard characterization techniques and EPR analysis, excitation-resolved photoluminescence (PL) spectroscopy. Their photocatalytic activity was also probed by standard methylene blue (MB) photo-degradation tests coupled with scavenging tests. The P25-GL composites exhibited an enhanced and spectrally-modified PL intensity, with a sharp decrease vs GL load. In more detail, it is observed that the presence of a small quantity of GL in the composite (1%) leads to a broad PL emission, in

which the NIR-PL of rutile phase in P25 becomes undetectable. Further increase in the GL content lead to an abrupt decrease to the PL intensity, while leaving unaffected the spectral shape. A slight improvement in the photocatalytic degradation rate of MB with respect to raw P25 is found for the composite containing the 1 wt.% of GL, suggesting that further GL loads do not improve the photocatalytic efficiency because of UV losses due to optical scattering and absorption by the GRM. Hole and ROS scavenging tests evidenced that the oxidation by reactive radicals formed from photo-excited electrons is negligibly affected by the presence of GL layers, while the oxidation by reactive radicals formed from photo-induced holes is hindered. These findings suggested that holes transfer from P25 to GL. Supposing that GL layers preferentially arrange themselves by covering the surface of secondary aggregates of P25 nanoparticles, they will act as interface between the  $\text{TiO}_2$  and the external environment. Partial transfer of photogenerated holes toward GL layers (Fig. 6, right panel) may determine a heterojunction effect (i.e. a built-in electrostatic potential profile) associated with the accumulation of mobile electrons (screening the hole excess in GL) and downward band-bending of the valence and conduction band edges [37]. This phenomenon differs from that occurring in the case of  $\text{TiO}_2/\text{rGO}$  composites (Fig. 6, left panel) where the electrons transfer from P25 conduction band to rGO (in agreement with the observed uniform and mild quenching of all the PL emission components of P25) [37].

These findings on  $\text{TiO}_2/\text{GL}$  composites represent useful basics to engineer future  $\text{TiO}_2/\text{GRM}$  heterojunctions and highlight the usefulness of PLE spectroscopy in studying charge transfer/separation in  $\text{TiO}_2$ -based composites.

#### 4. Conclusions

The focus of our approach is to set up carbon-based novel materials (from design to scale-up synthesis) for innovative applications, among them: CO<sub>2</sub> capture and storage (CCS), sensoristics, selective photo-oxidation, water remediation (heavy metals capture), bio-compatible interfaces and bio-inspired devices (ex. drug delivery, biomimetics). In our research we preferentially adopted wet-chemistry synthetic approaches, thanks to the possibility to finely tune the destructurement and the functionalization of the graphenic layers embedded in the carbonaceous matrix leaving the graphitic core untouched, thus preserving the conductive properties. We mostly use green solvents (water) and we focus on the development of cost-effective protocols exploiting the versatility of the carbonaceous moieties, prone to be modified (structuring/de-structuring) in mild condition at molecular level. A wide array of cost-effective carbon-based materials and composites have been designed, produced and characterized, with a particular care to the relationships between the nano-structuration and the macroscopic properties. These promising results encourage a feasible use of carbon black and related materials in the production of advanced materials with practical applications.

#### Acknowledgments

This paper is based on the collaboration with Alessandro Pezzella, Stefano Lettieri, Tiziana Polichetti, Francesco di Natale, Paola Ammendola, Raffaele Marotta, Luciana Lisi since many years.

#### References

- [1]. C.M. Long, M.A. Nascarella, P.A. Valberg, *Environ. Pollut.* 181 (2013) 271–286. DOI: [10.1016/j.envpol.2013.06.009](https://doi.org/10.1016/j.envpol.2013.06.009)
- [2]. A.Y. Watson, P.A. Valberg, *AIHA J.* 62 (2001) 218–228. DOI: [10.1080/15298660108984625](https://doi.org/10.1080/15298660108984625)
- [3]. M.M. Lounasvuori, D. Kelly, J.S. Foord, *Carbon* 129 (2018) 252–257. DOI: [10.1016/j.carbon.2017.12.020](https://doi.org/10.1016/j.carbon.2017.12.020)
- [4]. C-S. Wu, T-W. Chang, H. Teng, Y-L. Lee, *Energy* 115 (2016) 513–518. DOI: [10.1016/j.energy.2016.09.052](https://doi.org/10.1016/j.energy.2016.09.052)
- [5]. D. Liu, X. Zhao, L. Song, S. Zhang, *Ceram. Int.* 44 (2018) 13712–13719. DOI: [10.1016/j.ceramint.2018.04.212](https://doi.org/10.1016/j.ceramint.2018.04.212)
- [6]. O.A. Kokhanovskaya, G.I. Razdyakonova, V.A. Likholobov, *Procedia Engineer.* 152 (2016) 540–544. DOI: [10.1016/j.proeng.2016.07.652](https://doi.org/10.1016/j.proeng.2016.07.652)
- [7]. L.R. Pahalagedara, I.W. Siriwardane, N.D. Tissera, R.N. Wijesena, K.M. Nalin de Silva, *RSC Adv.* 7 (2017) 19174–19180. DOI: [10.1039/C7RA02184D](https://doi.org/10.1039/C7RA02184D)
- [8]. B. Chen, B. Li, Y. Gao, T-C. Ling, Z. Lu, Z. Li, *Constr. Build. Mater.* 144 (2017) 106–114. DOI: [10.1016/j.conbuildmat.2017.03.168](https://doi.org/10.1016/j.conbuildmat.2017.03.168)
- [9]. A.O. Monteiro, A. Loredò, P.M.F.J. Costa, M. Oeser, P.B. Cachim, *Constr. Build. Mater.* 154 (2017) 1079–1086. DOI: [10.1016/j.conbuildmat.2017.08.053](https://doi.org/10.1016/j.conbuildmat.2017.08.053)
- [10]. C. Arnal, M. Alfè, V. Gargiulo, A. Ciajolo, M.U. Alzueta, A. Millera, R. Bilbao, Characterization of Soot. 13 (333–362). In: Battin-Leclerc F., Simmie J., Blurock E. (eds) *Cleaner Combustion. Green Energy and Technology*. Springer, London. DOI: [10.1007/978-1-4471-5307-8\\_13](https://doi.org/10.1007/978-1-4471-5307-8_13)
- [11]. E. Santini, F. Ravera, M. Ferrari, M. Alfè, A. Ciajolo, L. Liggieri, *Colloid Surface A* 365 (1-3) (2010) 189–198. DOI: [10.1016/j.colsurfa.2010.01.041](https://doi.org/10.1016/j.colsurfa.2010.01.041)
- [12]. V. Gargiulo, M. Alfè, L. Lisi, C. Manfredi, S. Volino, F. Di Natale, *Water Air Soil Poll.* 228 (2017) 192–205. DOI: [10.1007/s11270-017-3378-5](https://doi.org/10.1007/s11270-017-3378-5)
- [13]. M. Alfè, P. Ammendola, V. Gargiulo, F. Raganati, R. Chirone, *Proc. Comb. Inst.* 35 (2015) 2801–2809. DOI: [10.1016/j.proci.2014.06.037](https://doi.org/10.1016/j.proci.2014.06.037)
- [14]. F. Raganati, M. Alfe, V. Gargiulo, R. Chirone, P. Ammendola, *Chem. Eng. Res. Des.* 134 (2018) 540–552. DOI: [10.1016/j.cherd.2018.04.037](https://doi.org/10.1016/j.cherd.2018.04.037)
- [15]. V. Gargiulo, M. Alfe, P. Ammendola, F. Raganati, R. Chirone, *Appl. Surf. Sci.* 360 (2016) 329–337. DOI: [10.1016/j.apsusc.2015.11.026](https://doi.org/10.1016/j.apsusc.2015.11.026)
- [16]. V. Gargiulo, M. Alfè, F. Raganati, A. Zhumagaliyeva, Y. Doszhanov, P. Ammendola, R. Chirone, *Combust. Sci. Technol.* 191 (2019) 1484–1498. DOI: [10.1080/00102202.2018.1546697](https://doi.org/10.1080/00102202.2018.1546697)
- [17]. A. Samanta, A. Zhao, G.K.H. Shimizu, P. Sarkar, R. Gupta, *Ind. Eng. Chem. Res.* 51 (2012) 1438–1463. DOI: [10.1021/ie200686q](https://doi.org/10.1021/ie200686q)
- [18]. D.M. D'Alessandro, B. Smit, J.R. Long, *Angew. Chem. Int.* 49 (2012) 6058–6082. DOI: [10.1002/anie.201000431](https://doi.org/10.1002/anie.201000431)
- [19]. P. Nugent, Y. Belmabkhout, S.D. Burd, A.J. Cairns, R. Luebke, K. Forrester, T. Pham, S. Ma, B. Space, L. Wojtas, M. Eddaoudi, M.J. Zaworotko, *Nat. Lett.* 495 (2013) 80–84. DOI: [10.1038/nature11893](https://doi.org/10.1038/nature11893)
- [20]. M. Oschatz, M. Antonietti, *Energy Environ. Sci.* 11 (2018) 57–70. DOI: [10.1039/C7EE02110K](https://doi.org/10.1039/C7EE02110K)
- [21]. J. Baltrusaitis, J.H. Jensen, V.H. Grassian, *J. Phys. Chem. B* 110 (2006) 12005–12016. DOI: [10.1021/jp057437j](https://doi.org/10.1021/jp057437j)
- [22]. A.K. Mishra, S. Ramaprabhu, *Energy Environ. Sci.* 4 (2011) 889–895. DOI: [10.1039/C0EE00076K](https://doi.org/10.1039/C0EE00076K)

- [23]. A.K. Mishra, S. Ramaprabhu, *J. Mater. Chem.* 21 (2011) 7467–7471. DOI: [10.1039/C1JM10996K](https://doi.org/10.1039/C1JM10996K)
- [24]. M. Alfè, V. Gargiulo, R. Di Capua, F. Chiarella, J.-N. Rouzaud, A. Vergara, A. Ciajolo, *ACS Appl. Mater. Interfaces* 4 (2012) 4491–4498. DOI: [10.1021/am301197q](https://doi.org/10.1021/am301197q)
- [25]. M. Alfè, V. Gargiulo, R. Di Capua, *Appl. Surf. Sci.* 353 (2015) 628–635. DOI: [10.1016/j.apsusc.2015.06.117](https://doi.org/10.1016/j.apsusc.2015.06.117)
- [26]. R. Di Capua, V. Gargiulo, M. Alfè, *Eurasian Chem. Tech. J.* 18 (2016) 263–274. DOI: [10.18321/ectj480](https://doi.org/10.18321/ectj480)
- [27]. V. Gargiulo, B. Alfano, R. Di Capua, M. Alfè, M. Vorokhta, T. Polichetti, E. Massera, M.L. Miglietta, C. Schiattarella, G. Di Francia, *J. App. Phys.* 123 (2018) 024503. DOI: [10.1063/1.5000914](https://doi.org/10.1063/1.5000914)
- [28]. L.J. Van Der Pauw, *Philips Res. Rep.* 13 (1958) 1–9.
- [29]. F.R. Baptista, S.A. Belhout, S. Giordani, S.J. Quinn, *Chem. Soc. Rev.* 44 (2015) 4433–4453. DOI: [10.1039/C4CS00379A](https://doi.org/10.1039/C4CS00379A)
- [30]. F. Villani, F. Loffredo, B. Alfano, M.L. Miglietta, L. Verdoliva, M. Alfè, V. Gargiulo, T. Polichetti «Graphene-like based-chemiresistors inkjet-printed onto paper substrate» submitted to Sensors and Microsystems: Proc. 19<sup>th</sup> AISEM 2017 National Conf. (Lecture Notes in Electrical Engineering): Leone, A., Forleo, A., Francioso, L., Capone, S., Siciliano, P., Di Natale, C. (Eds.)
- [31]. M. Singh, H.M. Haverinen, P. Dhagat, G.E. Jabbour, *Adv. Mater.* 22 (2010) 673–685. DOI: [10.1002/adma.200901141](https://doi.org/10.1002/adma.200901141)
- [32]. M. Olivi, M. Alfè, V. Gargiulo, F. Valle, F. Mura, M. Di Giosia, S. Rapino, C. Palleschi, D. Uccelletti, S. Fiorito, *J. Nanopart. Res.* 18 (12) (2016) 358. DOI: [10.1007/s11051-016-3673-x](https://doi.org/10.1007/s11051-016-3673-x)
- [33]. S. Liu, T.H. Zeng, M. Hofmann, E. Burcombe, J. Wei, R. Jiang, J. Kong, Y. Chen, *ACS Nano* 5 (2011) 6971–6980. DOI: [10.1021/nn202451x](https://doi.org/10.1021/nn202451x)
- [34]. M. Alfè, V. Gargiulo, L. Lisi, R. Di Capua, *Mater. Chem. Phys.* 147 (2014) 744–750. DOI: [10.1016/j.matchemphys.2014.06.015](https://doi.org/10.1016/j.matchemphys.2014.06.015)
- [35]. V. Gargiulo, M. Alfè, R.D. Capua, A.R. Togna, V. Cammisotto, S. Fiorito, A. Musto, A. Navarra, S. Parisi, A. Pezzella, *J. Mater. Chem. B* 3 (2015) 5070–5079. DOI: [10.1039/C5TB00343A](https://doi.org/10.1039/C5TB00343A)
- [36]. G.P. Papari, V. Gargiulo, M. Alfè, R. Di Capua, A. Pezzella, A. Andreone, *J. Appl. Phys.* 121 (2017) 145107. DOI: [10.1063/1.4980106](https://doi.org/10.1063/1.4980106)
- [37]. S. Lettieri, V. Gargiulo, D.K. Pallotti, G. Vitiello, P. Maddalena, M. Alfè, R. Marotta, *Catal. Today* 315 (2018) 19–30. DOI: [10.1016/j.cattod.2018.01.022](https://doi.org/10.1016/j.cattod.2018.01.022)
- [38]. M. Alfè, D. Spasiano, V. Gargiulo, G. Vitiello, R. Di Capua, R. Marotta, *Appl. Catal. Gen.* 487 (2014) 91–99. DOI: [10.1016/j.apcata.2014.09.002](https://doi.org/10.1016/j.apcata.2014.09.002)
- [39]. N. Stock, S. Biswas, *Chem. Rev.* 112 (2012) 933–969. DOI: [10.1021/cr200304e](https://doi.org/10.1021/cr200304e)
- [40]. J.-R. Li, J. Sculley, H.-C. Zhou, *Chem. Rev.* 112 (2012) 869–932. DOI: [10.1021/cr200190s](https://doi.org/10.1021/cr200190s)
- [41]. P. Horcajada, R. Gref, T. Baati, P.K. Allan, G. Maurin, P. Couvreur, G. Ferey, R.E. Morris, C. Serre, *Chem. Rev.* 112 (2012) 1232–1268. DOI: [10.1021/cr200256v](https://doi.org/10.1021/cr200256v)
- [42]. V. Stavila, A.A. Talin, M.D. Allendorf, *Chem. Soc. Rev.* 43 (2014) 5994–6010. DOI: [10.1039/C4CS00096J](https://doi.org/10.1039/C4CS00096J)
- [43]. T. Zhang, W. Lin, *Chem. Soc. Rev.* 43 (2014) 5982–5993. DOI: [10.1039/C4CS00103F](https://doi.org/10.1039/C4CS00103F)
- [44]. S.K. Bhardwaj, N. Bhardwaj, R. Kaur, J. Mehta, A.L. Sharma, K.-H. Kim, A. Deep, *J. Mater. Chem. A* 6 (2018) 14992–15009. DOI: [10.1039/C8TA04220A](https://doi.org/10.1039/C8TA04220A)
- [45]. M. Barra, I. Bonadies, C. Carfagna, A. Cassinese, F. Cimino, O. Crescenzi, V. Criscuolo, M. d’Ischia, M.G. Maglione, P. Manini, L. Migliaccio, A. Musto, A. Napolitano, A. Navarra, L. Panzella, S. Parisi, A. Pezzella, C.T. Prontera, P. Tassini, *MRS Advances* 1 (2015) 3801–3810. DOI: [10.1557/adv.2015.49](https://doi.org/10.1557/adv.2015.49)
- [46]. M. D’Ischia, K. Wakamatsu, A. Napolitano, S. Briganti, J.C. Garcia-Borron, D. Kovacs, P. Meredith, A. Pezzella, M. Picardo, T. Sarna, J.D. Simon, S. Ito, *Pigment Cell Melanoma Res.* 26 (2013) 616–633. DOI: [10.1111/pcmr.12121](https://doi.org/10.1111/pcmr.12121)
- [47]. R. Di Capua, V. Gargiulo, M. Alfè, G.M. De Luca, T. Skála, G. Mali, A. Pezzella, *Front. Chem.* 7 (2019) 121. DOI: [10.3389/fchem.2019.00121](https://doi.org/10.3389/fchem.2019.00121)
- [48]. S. Malato, P. Fernandez-Ibanez, M.I. Maldonado, J. Blanco, W. Gernjak, *Catal. Today* 147 (2009) 1–59. DOI: [10.1016/j.cattod.2009.06.018](https://doi.org/10.1016/j.cattod.2009.06.018)
- [49]. X. Chen, S.S. Mao, *Chem. Rev.* 107 (2007) 2891–2959. DOI: [10.1021/cr0500535](https://doi.org/10.1021/cr0500535)
- [50]. A. Ajmal, I. Majeed, R.N. Malik, H. Idriss, M.A. Nadeem, *RSC Adv.* 4 (2014) 37003–37026. DOI: [10.1039/C4RA06658H](https://doi.org/10.1039/C4RA06658H)
- [51]. R. Marschall, *Adv. Funct. Mater.* 24 (2014) 2421–2440. DOI: [10.1002/adfm.201303214](https://doi.org/10.1002/adfm.201303214)
- [52]. Y. Zhu, Y. Wang, W. Yao, R. Zong, Y. Zhu, *RSC Adv.* 5 (2015) 29201–29208. DOI: [10.1039/C5RA02458G](https://doi.org/10.1039/C5RA02458G)